SYNCHROTRON RADIATION APPLICATION FOR LATTICE STRAIN MEASUREMENTS

Elżbieta Gadalińska[1]
Andrzej Baczmański[2]
Kamil Sołoducha[2]

[1]*Institute of Aviation, Al. Krakowska 110/114, 02-256 Warsaw, Poland*
[2] *AGH-University of Science and Technology, WFIS, Al. Mickiewicza 30, 30-059 Kraków, Poland*

elzbieta.gadalinska@ilot.edu.pl, andrzej.baczmanski@fis.agh.edu.pl, kamil.soloducha@fis.agh.edu.pl

Abstract

The methods most commonly used for the determination of the elastic lattice deformation and distortion are diffraction methods, which enable to perform measurements of stresses and elastic properties of polycrystalline materials. The main advantages of diffraction methods are associated with their non-destructive character and the possibility to be used for macrostress and microstress analysis of multiphase and anisotropic materials. Diffraction methods enable taking measurements selectively only for a chosen alloy phase. This is very convenient when several phases are present in the sample since measurements of separate diffraction peaks allow the behaviour of each phase to be investigated independently.

In this work, a method for analysis of diffraction with synchrotron radiation is described. The methodology is based on the measurements of lattice strains during "in situ" tensile testing for several hkl reflections and for different orientations of the sample with respect to the scattering vector. Some initial results are presented.

Keywords: *diffraction, synchrotron radiation, lattice strain, micromechanical properties of duplex steel, in situ tensile test*

METHODOLOGY

Classification of stress types in polycrystalline materials

As an effect of technological treatment and processing of a material, or thermal treatment of two-phase composites (different thermal expansion coefficient of every individual composite phase causes a different strain to appear in every phase), the residual stresses may appear. These stresses are defined as derivate of elastic strains that remained after the technological treatment and processing of the material. Residual stresses remain in the material even after specimen lightening (e.g. in the case of plastic deformation). They remain in the material when the surface of the specimen was deformed to a considerably greater extent than the inner part of the specimen. Another reason for the occurrence of residual stresses is the laser treatment of the surface.

There are three types of residual stresses. Stresses of first order represent these for a relatively big part of the specimen, for big amount of grains. Their value does not depend on the position of the measurement point. First-order stresses appear e.g. in rolled specimens where a component appears which is parallel and perpendicular to the rolling direction. Second-order stresses change

from grain to grain. They can be observed in rolled specimens, too. Second-order stresses originate from different plastic deformations of an individual grain. Third-order stresses' values change inside every single grain. This type of stresses originates from dislocations or grain boundaries. The average value of second and third-order stresses in the whole volume of the grain is zero.

The effect of residual strain and stress on the diffraction image

Diffraction methods are very convenient for the investigation of the residual stress state. This is due to the fact that the effect of the lattice strain on the position of diffraction peaks or changes its full width at half maximum (FWHM). The first and second-order stresses cause a systematic shift of diffraction peaks on the intensity vs. 2Θ graph (Fig. 1). Diffraction peaks originate from many grains so the information about measured strain is averaged out. It is important to note that not every grain gives diffraction peaks, but only these with the appropriate orientation and which satisfy Braggs' law. The third-order stresses originate from dislocations of the atoms (atoms are not placed in their nodes) (Fig. 2a). This causes the diffraction peaks to broaden (Fig. 2b). The same phenomenon appears for specimens made of material with a different grain size. There are some methods (Sherrer or Williamson-Hall formulas) which enable calculating the grain size from the broadening of diffraction peak.
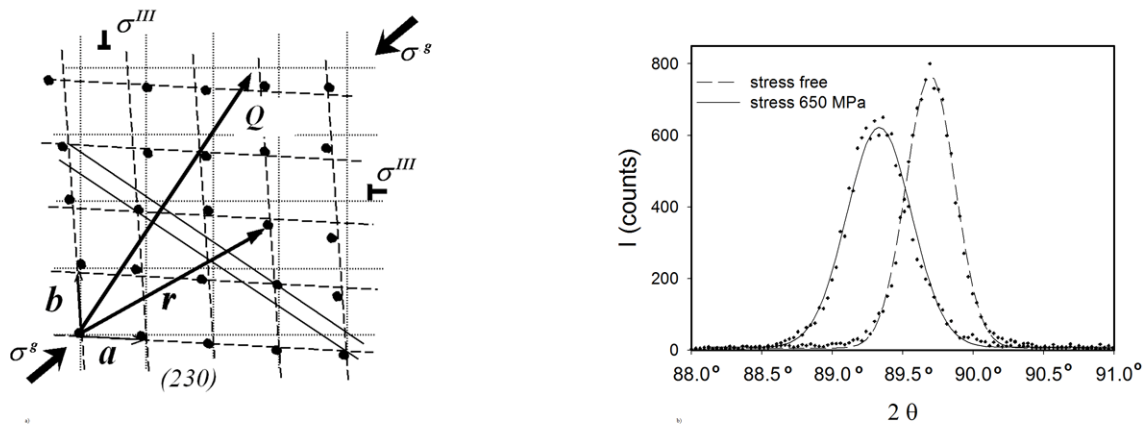

***Fig. 1. Deformation of the crystal lattice in case of first and second order stresses (a)
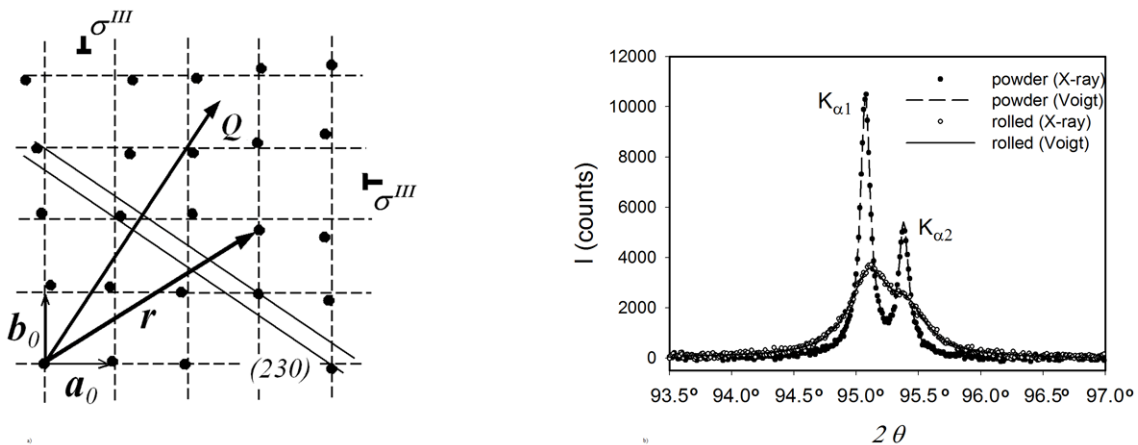and its influence on the position of diffraction peaks (b)***

***Fig. 2. Deformation of the crystal lattice in case of third order stresses (a)
and its influence on the broadening of diffraction peaks (b)***

Figure 3. shows the relation between the change in inter-planar distances and the value of Braggs' angle. When the specimen is stretched, inter-planar distances grow (Fig. 3a,b). This causes Braggs' angle to decrease and diffraction peak to shift (Fig. 3c).
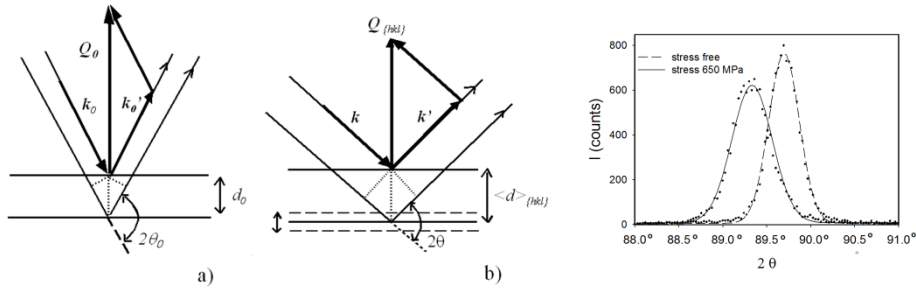

Fig. 3. Relation between the change of inter-planar distances and the value of the Braggs' angle

It is very important to notice that diffraction occurs only for grains for which the scattering vector is perpendicular to *hkl* planes (the darkest grains in the Fig. 4).
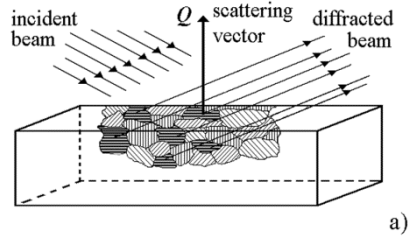

Fig. 4. X-ray diffraction for grains which hkl planes are perpendicular to the scattering vector

Exact strain values can be obtained employing two basic equations 1 and 2:

$$n\lambda = 2d_{hkl} \sin \Theta$$ (eq. 1)

Where:
n – natural number,
λ – wavelength of the X radiation used in the experiment,
d_{hkl} – inter-planar distance for the specimen after deformation,
Θ – Bragg's angle.

The definition of strain is as follows:

$$\langle \varepsilon \rangle_{hkl} = \frac{\langle d \rangle_{hkl} - d_{hkl}^0}{d_{hkl}^0}$$ (eq. 2)

Where:
$\langle \varepsilon \rangle_{hkl}$ – average strain for grains taking part in diffraction, for *hkl* planes, for deformed material,

$\langle d \rangle_{hkl}$ – average inter-planar distances for *hkl* planes, for deformed material,

d_{hkl}^0 – inter-planar distances for *hkl* planes, for undeformed material

After measuring strain values for selected grains, stress values can be obtained with the following equation:

$$\left\langle \varepsilon\left(\varphi,\psi\right)\right\rangle_{hkl} = F_{ij}(hkl,\varphi,\psi)\sigma_{ij}^{I} \qquad \text{(eq. 3)}$$

Where:

$\left\langle \varepsilon(\varphi,\psi)\right\rangle_{hkl}$ – the average value of strain for *hkl* planes, direction defined by φ and ψ angles,

$F_{ij}(hkl,\varphi,\psi)$ – diffraction elastic constants for *hkl* planes, direction defined by φ and ψ angles; values which depend on the Miller indices *hkl* and the φ and ψ angles. Values of the diffraction elastic constants can be known as a result of appropriate experiment or modeling,

σ_{ij}^{I} – first-order stress values,

φ – angle between the direction of measured strains and the preferable axis of the specimen, first angle which defines the orientation of the scattering vector,

ψ – angle between the scattering vector and the surface perpendicular to the specimen surface, second angle which defines the orientation of the scattering vector.

Synchrotron radiation and its application in residual stress measurements

Every charged particle accelerated or decelerated emits the electromagnetic wave. This phenomenon can be observed in two main cases. In the first case the velocity change is joined with rectilinear motion and the particle is decelerated while in the second case the charged particle is accelerated radially (a⊥v). In the latter case synchrotron radiation is produced. Depending on the particle's energy, the spectrum of synchrotron radiation can vary from high energy radiation to infrared radiation. The radiation produced by high-energy particles is extensively collimated tangentially to the particle's trajectory. It is linearly polarized in the plane of the particle's motion. At the end of the beam, circular polarization is observed. The synchrotron radiation impulses last only few picoseconds and are repeated every 1ns - 1μs. The spectrum of radiation produced is continuous but it is possible to cut/single out a very narrow radiation range of the wavelength of interest for the researcher and to obtain monochromatic radiation. For X radiation, the intensity of synchrotron radiation is higher by few orders of magnitude than in the case of X radiation produced by X-ray tubes. Depending on the wavelength, synchrotron radiation can be a very useful tool for investigating materials in solid state. It can be used for investigation of crystalline as well as amorphous materials. High-energy radiation can be applied to carry out strain measurements. Additionally, the application of synchrotron radiation with the wavelength beam of 0,1μm enables researchers to obtain information about strain for an individual grain or inside a single grain. To summarize, synchrotron radiation is useful when the measurement is meant to be performed in the volume inside the material and the examined volume is expected to be relatively narrow (see Fig. 5, the diamond shape measured volume can be even few micrometers). Additionally, synchrotron radiation allows strain measurements to be carried out much more faster and with better resolution than in the case of X radiation.
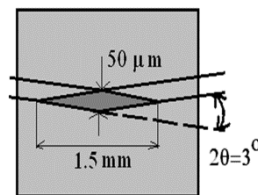

Fig. 5. Examined volume and its shape for synchrotron radiation

The most popular mode for synchrotron radiation is the transmission mode (Fig. 6). The Debeye-Sherrer rings are observed on the two-dimensional detector.
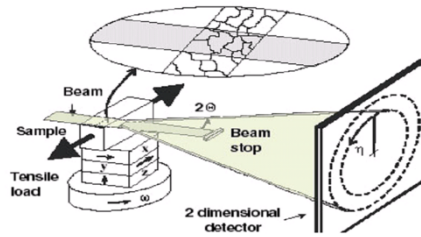

Fig. 6. Transmission mode for synchrotron radiation

ESRF EXPERIMENT AND SOME RESULTS

The ESRF synchrotron and the experiment

The experiment was performed at the European Synchrotron Radiation Facility (ESRF), Grenoble, France. Figure 7 below presents the synchrotron scheme with beamlines indicated. The experiment was performed on beamline 15b with the monochromatic wave dedicated to polycrystalline materials.
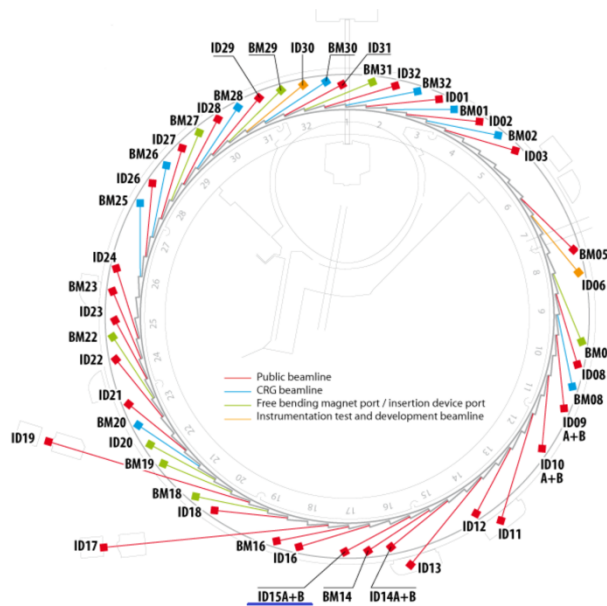

Fig. 1 The ESRF synchrotron scheme

Beamline15b is dedicated to diffraction experiments of powder specimens, amorphous materials and single crystals. The electromagnets employed on beamline number 15b are able to generate the magnetic field of 8T magnetic induction. A special apparatus is used to apply forces equal to 50kN. The beams are of three different energies: 30 keV, 60 keV and 90 keV. It is possible due to monochromators attached. The beam size can change; the minimal possible cross section is $50\mu m$ x $50\mu m$ and the maximal is $6mm$ x $6mm$. The research data was obtained from the experiment conducted for the two phase (austenite and ferrite) steel. The presence of two phases in this alloy causes the appearance of unique advantages. Austenite phase increases ductility and the ferritic phase increases hardness and strength.
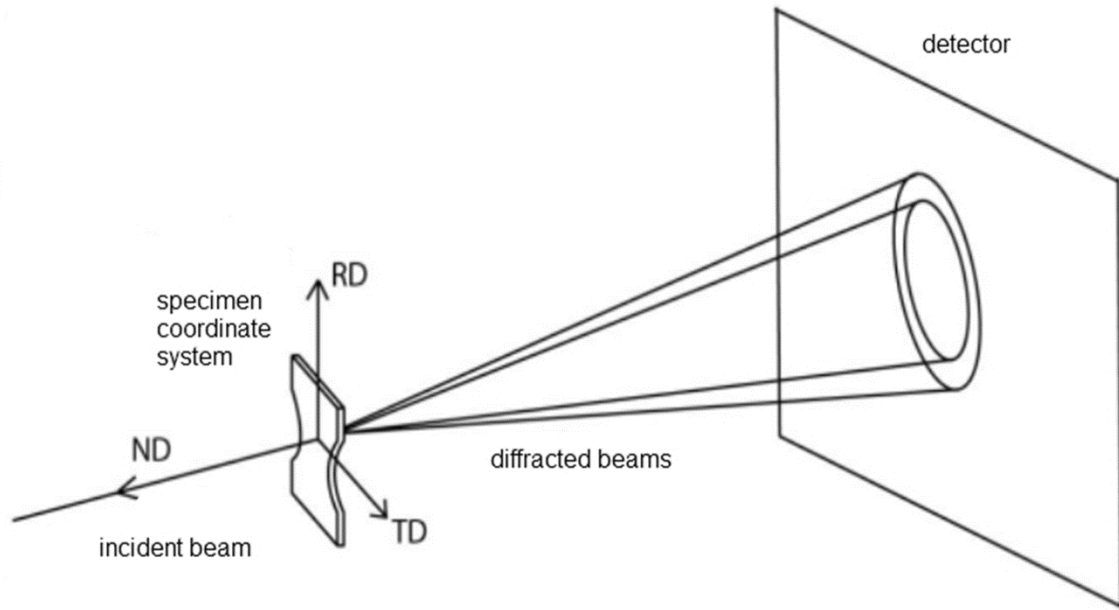
Fig. 8. Transmission mode of the diffraction experiment

The experiment involved measuring the lattice strain of the specimen made of duplex steel with diffraction of synchrotron radiation. The specimen was subjected to the one axis tensile test. Applied force caused stresses of the first and second order. The diffraction image was recorded over one hundred times during the experiment. The radiation applied in the experiment was the synchrotron radiation with the wavelength of $\lambda = 0,14256\ \mathring{A}$, and the beam cross-section of $100\mu m$ x $100\mu m$. After diffraction on the crystallographic planes, the diffracted beam was detected on the CCD detector. The detector was $345mm$ x $345mm$ square. The distance between the specimen and the detector was $897,551mm$. The output data were diffraction images saved as a bitmap of size 2640 x 1920 pixels. The diffraction image was recorded every 10 seconds.
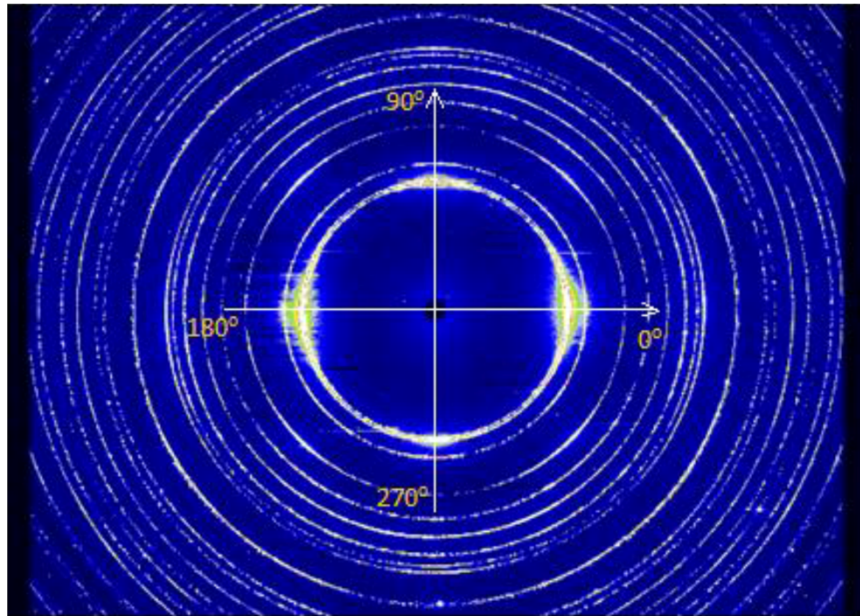

Fig. 9. ESRF synchrotron diffraction image

RESULTS

The initially obtained results showed a certain degree of disagreement between the experimental results and the model, which was most probably due to the existence of initial stresses in the specimen. The values of initial stresses were predicted with the $sin^2\psi$ method and are given below.

$$\sigma_{ij\ austenite} = \begin{bmatrix} -49,7 & 0 & 11,3 \\ 0 & -352,4 & -9,3 \\ 11,3 & -9,3 & 0 \end{bmatrix}$$

$$\sigma_{ij\ ferrite} = \begin{bmatrix} 111,3 & 0 & 1,6 \\ 0 & 355,1 & 30,7 \\ 1,6 & 30,7 & 0 \end{bmatrix}$$

Taking into account the right values of initial stresses and correcting the original values of τ_{cr} and H we were able to predict the material behavior when the force was applied to it. Experimental results in comparison with the model are presented in Fig. 10 and 11 while the correct τ_{cr} and H values are given in Table 1.

	phase	$C_{11}(GPa)$	$C_{121}(GPa)$	$C_{44}(GPa)$	$\tau_c^s(MPa)$	$H(MPa)$
modeling without initial stresses	austenite	198	125	122	50	255
	ferrite	231	134	116	550	130
modeling with initial stresses	austenite	198	125	122	140	255
	ferrite	231	134	116	450	130

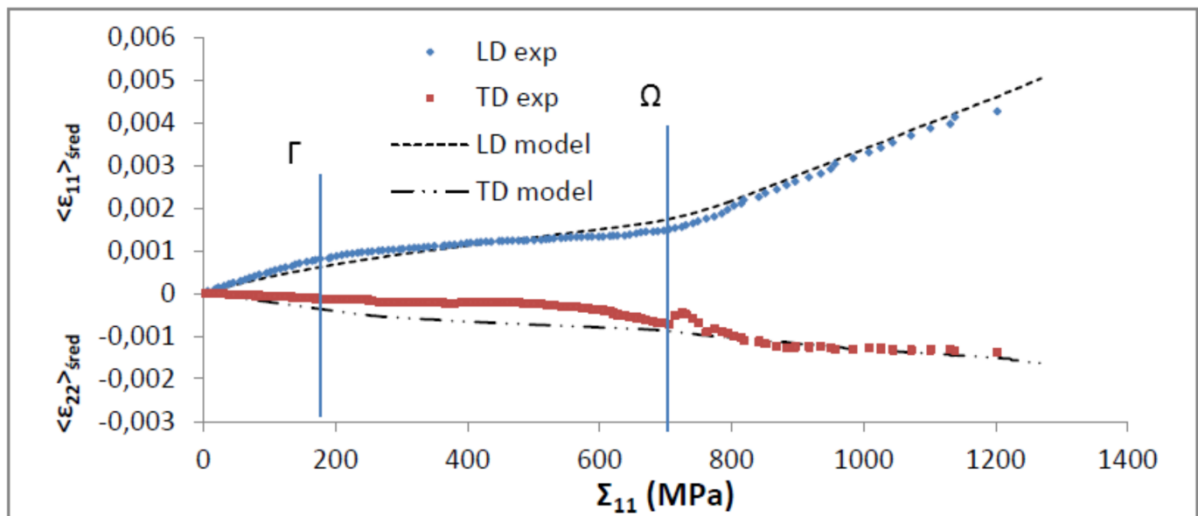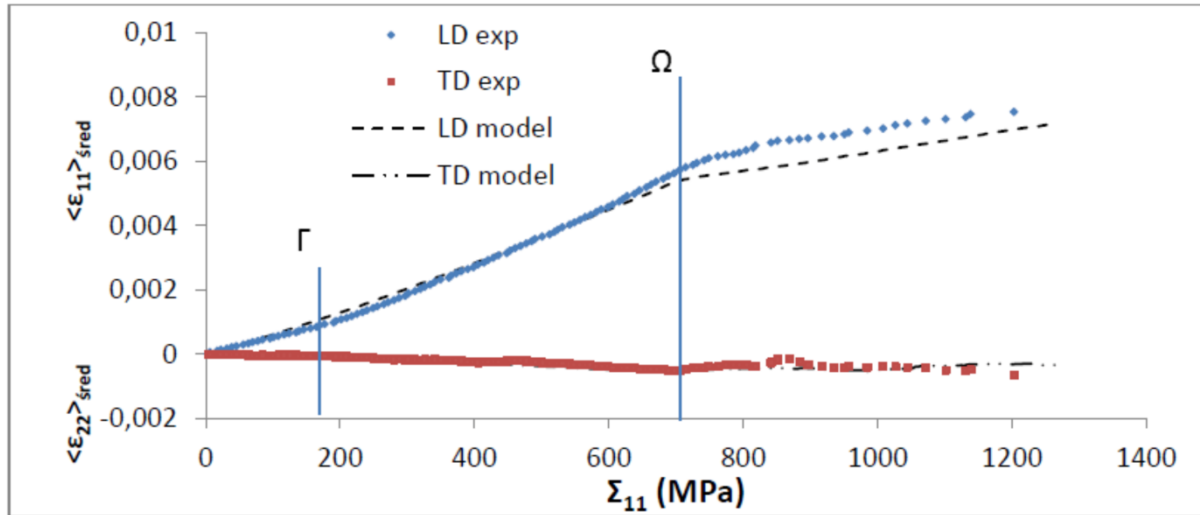*Table 1. Initial and corrected material data*

Fig. 10. Model and experimental relations $\langle\varepsilon_{11}\rangle$ and $\langle\varepsilon_{11}\rangle vs. \Sigma_{11}$
after initial stresses were taken into account – austenitic phase

***Fig. 2 Model and experimental relations ⟨ε_11 ⟩ and ⟨ε_11 ⟩ vs. Σ_11
after initial stresses were taken into account – ferritic phase***

It was found that the initial stresses significantly changed the critical shear stre0073s τ_{cr} for both phases. Meanwhile, the hardening parameter value H remained unchanged for ferrite as well as for austenite. Below, different peaks are plotted for the austenitic and ferrite phase separately.
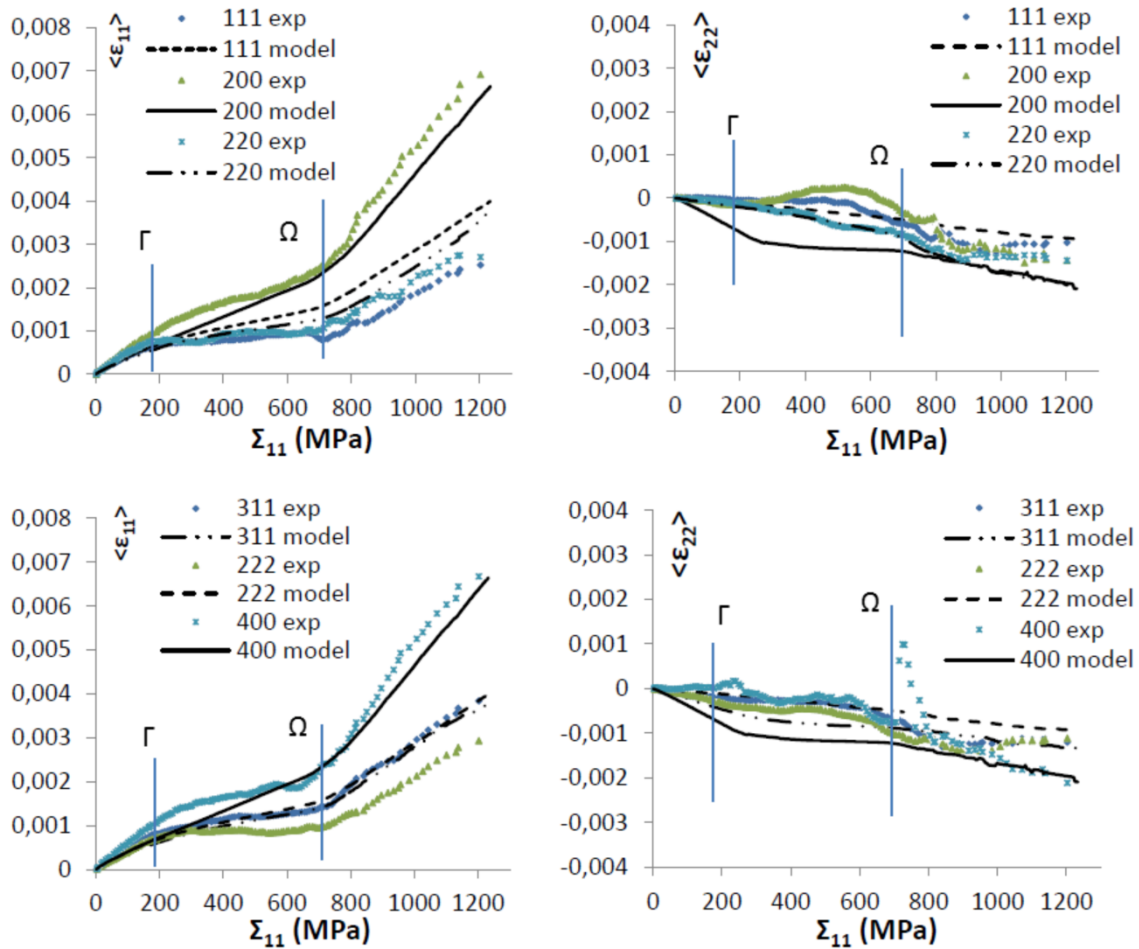

***Fig. 3 Strain vs. macrostress for the austenitic phase.
Two upper plots are for LD direction, lower ones for TD direction***

A very good agreement between the experimental results and the model was observed for the LD direction after the initial stresses were taken into account (Fig. 12). Only for peaks (111) and (222) there was a significant discrepancy between the experimental data and the model. On every plot it is possible to observe the yield point of the material (Γ and Ω points). For the second direction i.e. TD direction, the agreement between the experiment and the model was the least satisfactory. Good agreement could be observed for peak with *hkl* (220) until the stress value equal to 900MPa.
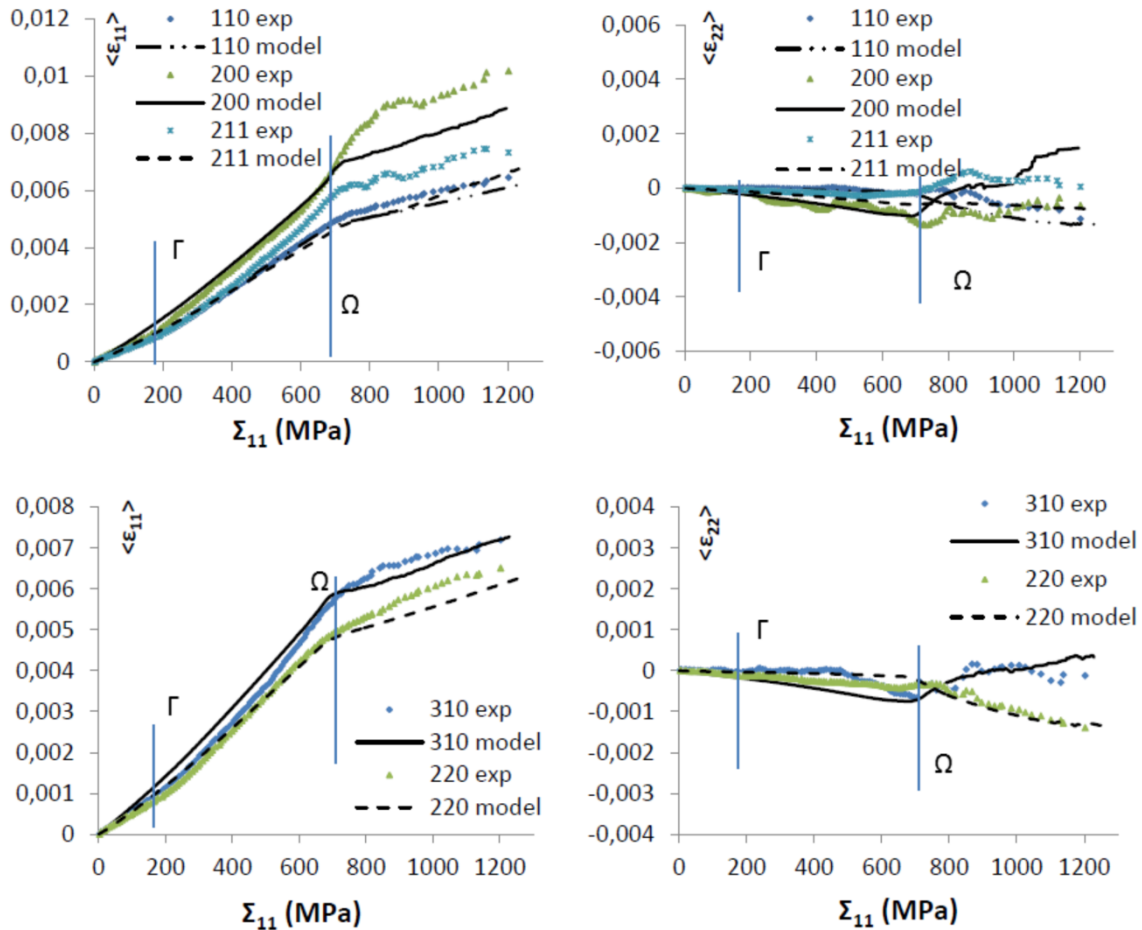

Fig. 4 Strain vs. macrostress for the ferritic phase.
Two upper plots are for LD direction, lower ones for TD direction

In the case of ferrite there was good agreement between the experiment and the model for the LD direction (Fig. 13). However, for the plastic range of strain, the experimental data and the modeling results diverged for peaks (200) and (211). For the TD direction the model and the experimental results agreed well.

CONCLUSIONS

The aim of the work was to analyze and interpret the results of the diffraction experiment performed for the two-phase steel during in situ tensile testing in transmission mode. The main goal was to show the relation between the material strain and the applied macrostress. The yield point for separate phase of the material can be read from the plots. The comparison of the plots for the austenitic and ferritic phase shows the dependence between these phases during the elasto-

plastic deformation process. The modeling trials show that the model fits experimental data very well only when the initial stresses are taken into account. The plots of the relation $\langle \varepsilon \rangle$ vs. Σ_{11} that included the initial stresses showed a better agreement between the experimental data and modeling results. The significant difference was observed in the τ_{cr} value when the initial stresses were taken into account and when they were not. It means that the residual stress state affects a yield point of both ferrite and austenite.

The relation between lattice strain and stress applied to the specimen was presented. It can be concluded that for the elastic range of strain the model results fitted the experimental data very well. It was observed that when the material went into a plastic range of strain this agreement deteriorated. The reason of this phenomenon can be a symptom of an anisotropic stress state in each phase (in other words: about the presence of second order stresses).

ACKNOWLEDGEMENTS

REFERENCES

1. Kisiel, A. (2006). Synchrotron jako narzędzie: zastosowania promieniowania synchrotronowego w spektroskopii ciała stałego. *Synchrotron Radiation in Natural Science*, Vol. 5, No 3.
2. http://www.esrf.eu/
3. Lipinski, P., Berveiller, M., (1989). Elastoplasticity of micro-inhomogeneous metals at large strains. *Int. J. Plastic*. 5, pp. 149–172.
4. A. Baczmański, L. Le Joncour, B. Panicaud, M. Francois, C. Braham, A. M. Paradowska, S. Wrooski, S. Amara and R. Chirone (2011). Neutron time-of-flight diffraction used to study aged duplex stainless steel at small and large deformation until sample fracture. *Journal of Applied Crystallography*, 44, pp. 966-982.
5. Baczmański, A., Lipinski, P., Tidu, A., Wierzbanowski, K. and Pathiraj B. (2008). Quantitative estimation of incompatibility stresses and elastic energy stored in ferritic steel, *J. Appl. Cryst*, 41, pp. 854–867.